Qiang Zhang
Research Assistant Professor

Matt Goodro
Undergraduate Research Assistant

Phillip M. Ligrani[1]
Professor
ASME Fellow

Convective Heat Transfer Laboratory,
Department of Mechanical Engineering,
University of Utah,
Salt Lake City, Utah 84112-9208

Ricardo Trindade
Staff Engineer
Turbine Durability,
United Technologies,
Pratt and Whitney Corp.,
400 Main Street, M/S 169-29,
East Hartford, CT 06108

Sri Sreekanth
Principle Engineer
Turbine Cooling and Static Structures,
Pratt and Whitney – Canada Corp. 22MC1,
1801 Courtney Park Drive East,
Mississauga, Ontario L5T1J3, Canada

Influence of Surface Roughness on the Aerodynamic Losses of a Turbine Vane

The effects of surface roughness on the aerodynamic performance of a turbine vane are investigated for three Mach number distributions, one of which results in transonic flow. Four turbine vanes, each with the same shape and exterior dimensions, are employed with different rough surfaces. The nonuniform, irregular, three-dimensional roughness on the tested vanes is employed to match the roughness which exists on operating turbine vanes subject to extended operating times with significant particulate deposition on the surfaces. Wake profiles are measured for two different positions downstream the vane trailing edge. The contributions of varying surface roughness to aerodynamic losses, Mach number profiles, normalized kinetic energy profiles, Integrated Aerodynamics Losses (IAL), area-averaged loss coefficients, and mass-averaged loss coefficients are quantified. Total pressure losses, Mach number deficits, and deficits of kinetic energy all increase at each profile location within the wake as the size of equivalent sandgrain roughness increases, provided the roughness on the surfaces is uniform. Corresponding Integrated Aerodynamic Loss IAL magnitudes increase either as Mach numbers along the airfoil are higher, or as the size of surface roughness increases. Data are also provided which illustrate the larger loss magnitudes which are present with flow turning and cambered airfoils, than with symmetric airfoils. Also described are wake broadening, profile asymmetry, and effects of increased turbulent diffusion, variable surface roughness, and streamwise development.
[DOI: 10.1115/1.2175163]

1 Introduction

Turbomachinery efficiency and operational behavior are influenced in important ways by the surface roughness of the turbine vanes and blades. This paper presents experimental results which illustrate the effects of roughness on the aerodynamic losses produced by cambered turbine vanes, both with and without different types of surface roughness, operating over a range of flow conditions which match those used in industrial applications.

The influence of surface roughness on adjacent flow behavior has been of interest for researchers for almost 100 years. The use of equivalent sandgrain roughness size k_s to characterize and quantify rough surfaces was first proposed and utilized by Nikuradse [1] and Schlichting [2]. This quantity represents the size of sand grains which give the same skin friction coefficients in internal passages as the roughness being evaluated. This measure of roughness size continues to be used widely in empirical correlation equations (which are based on experimental data) to represent rough surface behavior, and for closure models employed in a variety of numerical prediction codes. Later re-evaluation and additional advances in the use of equivalent sandgrain roughness are made by many researchers, including Coleman et al. [3], Sigal and Danberg [4,5], Van Rij et al. [6] and Zhang et al. [7].

In a paper published in 1975, Bammert and Sandstede [8] describe the influences of different manufacturing tolerances and turbine airfoil surface roughness characteristics on the overall performance of turbines. Particular attention is devoted to the effects of these parameters on efficiency, relative mass flow, enthalpy drop, and outlet flow angle. Later work by the same authors [9] considers the effects of the surface roughness on the boundary layer development along blades arranged in a stationary cascade. Momentum thicknesses are as much as three times values measured on smooth airfoils in regions of decelerating flow. Kind et al. [10] investigate the effects of partial roughness coverage of blade surfaces by measuring pressure distributions, profile losses, and the flow deviations produced by a planar turbine cascade. Different roughness heights, and different roughness element spacings are considered. According to the authors, the largest profile loss increases are produced by roughness located on the suction surface. Bogard et al. [11] analyze the surface roughness characteristics of turbine vanes that have undergone a significant number of hours of operation. Flat plate surfaces with cone shaped elements are used to simulate the roughness which is present on these vane surfaces. According to the authors, the effects of surface roughness and high free-stream turbulence are additive along flat plates, and can produce heat transfer rate increases that are as much as 100% greater than smooth surface values. Abuaf et al. [12] quantify heat transfer and aerodynamics performance characteristics of turbine airfoils with different surface finish treatments. Experimental results show that tumbling and polishing reduce the average roughness size and improve overall performance. The authors also employ a Reynolds analogy to determine skin friction coefficients, drag forces, and aerodynamic efficiencies from airfoil surface heat transfer data. Leipold et al. [13] employ a compressor cascade to investigate the influences of surface roughness at different inlet flow angles and Reynolds numbers. The investigators indicate that surface roughness has no effect upon the presence or location of laminar separation, and that the roughness alters turbulent boundary layer separation at high Reynolds numbers.

[1]Corresponding author.

Contributed by the Fluids Engineering Division of ASME for publication in the JOURNAL OF FLUIDS ENGINEERING. Manuscript received February 3, 2005; final manuscript received October 16, 2005. Review conducted by Joseph Katz. Paper presented at the TURBO EXPO 2005 in Reno.

The investigation by Sitaram et al. [14] attempts to reduce losses by reducing the laminar separation bubble on the suction surface of a turbine rotor blade by means of a two-dimensional roughness element. Experimental data on wake pressure defects, velocity, flow angle, and wake decay characteristics are obtained. They conclude that blade static pressure distributions are little altered by surface roughness on suction surfaces. Combined effects of surface roughness, freestream turbulence and Reynolds number on heat transfer and laminar-turbulent transition are investigated by Stripf et al. [15]. Their results show a strong influence of roughness on the onset of transition even for the smallest roughness Reynolds numbers. Roberts and Yaras [16] also present experimental results showing that transition inception location remains sensitive to surface roughness with increasing freestream turbulence.

Boyle and Senyitko [17] compare total pressure losses for smooth and rough vanes over a range of Reynolds and Mach numbers for three turbulence levels. Their work concentrates on loss differences between the rough and smooth vanes, and on approaches to predicting surface roughness effects. They indicate that, at high Reynolds numbers, roughness nearly doubles loss levels compared to ones which exist for the lowest Reynolds number employed. The effects of surface roughness on the aerodynamic performance of symmetric airfoils are investigated by Zhang et al. [18] with different inlet turbulence intensity levels. Their results show that effects of changing the size of surface roughness on the Integrated Aerodynamic Losses (IAL) are substantial, whereas the effects of different inlet turbulence intensity levels are generally relatively small. In another study, Zhang et al. [19] present experimental data on wake turbulence structure also measured downstream of symmetric airfoils with different surface roughness and inlet turbulence intensity levels. These authors indicate that all wake profile quantities broaden and vortex shedding frequencies decrease as either the level of surface roughness or the turbulence intensity increases. Note that significant flow turning from a cambered airfoil is not present in these two investigations by Zhang et al. [18,19].

The present investigation is different from the investigations of Zhang et al. [7,18,19] because a cambered turbine vane is used which produces substantial flow turning, and matches a vane configuration employed in an industrial application. Considered are the effects of surface roughness on aerodynamic losses downstream of the vane for three different Mach number distributions, one of which results in transonic flow (and matches flow conditions in an industrial application). One smooth vane is employed, along with two other vanes with three-dimensional roughness distributed uniformly over entire vane surfaces. A fourth vane is also employed with roughness of different sizes distributed over the vane surface (i.e., a variable rough surface) whose arrangement is based on observations of roughened turbine vanes from industrial applications. All four turbine vanes have the same shape and exterior dimensions. These aspects of the present approach make the present investigation unique and different from other investigations of turbine airfoil aerodynamic losses. As such, the data provide useful information to designers of turbomachinery components for evaluation of turbine efficiency, and to individuals developing models for CFD predictions. Wake profile data are presented for two different locations downstream the vane trailing edge, which illustrate the influences of varying surface roughness and vane Mach number on local aerodynamic losses, local Mach numbers, local kinetic energy, Integrated Aerodynamics Losses (IAL), area-averaged loss coefficients, and mass-averaged loss coefficients. Included are comparisons with results from several other recent investigations [10,17,20–22].

2 Experimental Apparatus and Procedures

2.1 Transonic Wind Tunnel (TWT). The University of Utah Transonic Wind Tunnel (TWT) is used for the study because it produces Mach numbers, pressure variations, Reynolds numbers, passage mass flow rates, and scaled physical dimensions which match values along airfoils in operating aero-engines and in gas turbines used for utility power generation. The TWT blow-down type facility consists of two main parts: (i) compressor and storage tanks, and (ii) wind tunnel. The wind tunnel consists of five major sub-sections: (i) flow rate and pressure level management apparatus, (ii) plenum tank, (iii) inlet ducting and test section, (iv) plenum, exit ducting, and ejector, and (v) control panel. Detailed descriptions are provided by Jackson et al. [23] and Furukawa and Ligrani [24].

Table 1 Operating conditions

Exit Mach number M_{ex}	0.35	0.50	0.71
Exit Reynolds number*	0.5×10^6	0.7×10^6	0.95×10^6
Inlet Reynolds number*	0.2×10^6	0.3×10^6	0.4×10^6
Inlet Mach number	0.15	0.19	0.23
Inlet Total Pressure (kPa)	94	98	106
Inlet Turbulence Intensity	1.6%	1.2%	1.1%
Inlet Relative humidity	15-20%	15-20%	15-20%

A Gardner-Denver Co. model RL-1155-CB compressor is used to pressurize the array of eight tanks whose total capacity volume is 11.9 m^3. A VanAir VAS93039 model D16-5 Deliquescent desiccant dryer, a Pall Corp. 5EHG-4882-207 oil filter, and two Permanent Filter Corp. No. 13846 particulate filters are located just downstream of the compressor to remove particulates and moisture from the air. A Fisher pressure regulator with a 6×4 EWT design sliding gate valve, a Fisher type 667 diaphragm actuator, a 3582 series valve positioner, and a Powers 535 1/4 DIN process controller are used to regulate the pressure in the test section as the storage tanks discharge. A plenum tank, a 30.48 cm inner diameter pipe, a circular-to-square transition duct, a nozzle, and the test section then follow. The test section is connected to a large 92.71 cm by 91.44 cm by 91.44 cm plenum with a square plastic flange at its outlet. The plenum diffuses high speed air from the test section exit into a reservoir of low velocity air. This plenum is then connected to two ducts which are subsequently connected to the atmosphere.

Experimental parameters for the three different operating conditions employed in this study are tabulated in Table 1.

2.2 Test Section. The present test section is designed to match Reynolds numbers, Mach numbers, pressure gradients, passage mass flow rates, boundary layer development, streamline curvature, airfoil camber, and physical dimensions of turbine vanes in operating industrial engines. A schematic diagram of the test section with the cambered vane is shown in Fig. 1, along with the *x*-*y* coordinate system used for wake profile measurements. The inlet of the test section is 12.70 cm by 12.70 cm. The side and bottom walls of the test section are made of steel, and top wall is made up of acrylic. As shown in Fig. 1, two zinc-selenide windows are also placed on both of the sidewalls, so that the entire airfoil surface is accessible to optical, surface temperature measurement schemes such as infrared thermography.

Appropriate cascade flow conditions are maintained, in part, by a pair of adjustable bleed ducts which are located on the two side walls, as shown in Fig. 1. The flow rate of each bleed duct is regulated using an adjustable ball valve. Following these, the test section walls have the same pressure side and suction side contours as the test vane. The exit area and exit flow direction from the cascade test section can be altered by changing the angles of the two exit tailboards, which are also shown in Fig. 1. Thus, (i)

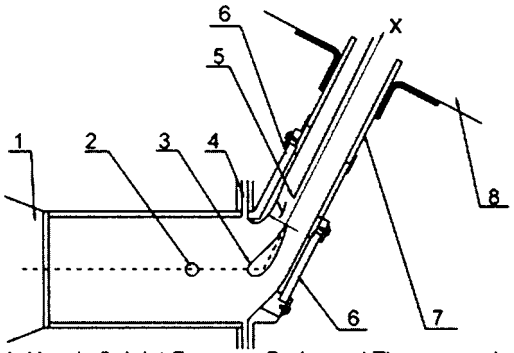

Fig. 1 Schematic diagram of the test section, including wake coordinate system

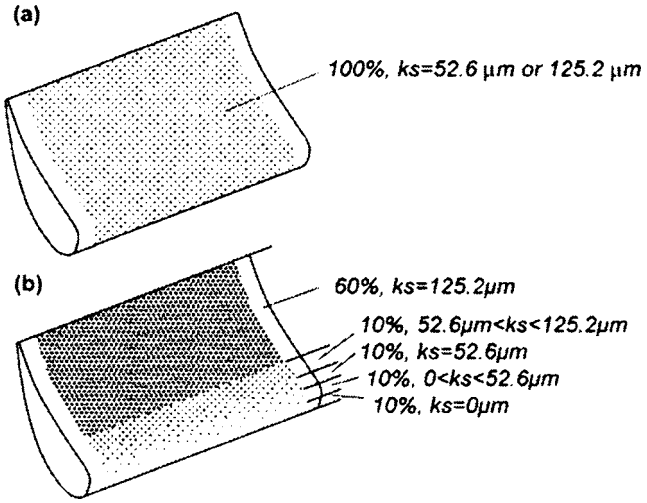

Fig. 2 Test section vanes with rough surfaces. (*a*) Vane with uniform roughness. (*b*) Vane with variable roughness on pressure side.

changing the total pressure at the test section inlet using the pressure regulator/sliding gate valve arrangement; (ii) changing the angular positions of the two tailboards; and (iii) adjusting the ball valves of the bleeding system are employed to alter the Mach number distribution along the vane in the test section, for a particular vane and test section configuration. By adjusting these items, appropriate Mach number distributions along the test vane are obtained, which are discussed later in the paper.

2.3 Test Vanes and Surface Roughness. Table 2 gives geometric parameters of the test vanes. The coordinates of this test vane profile were provided by personnel at Pratt and Whitney Canada Corporation, along with appropriate operating conditions which are used in industrial environments.

Four different vanes, all with the same exterior dimensions but with different surface roughness characteristics, are used. One vane has a smooth surface, two other vanes have uniform rough surfaces, and one vane has variable roughness on the pressure side. The roughness applied simulates the actual roughness which develops on operating turbine airfoils, over long operating times, due to particulate deposition and to spallation of thermal barrier coatings (TBCs). The roughness is applied by bonding nickel particles, manufactured by Praxair Surface Technologies, Inc., to the test vane surfaces. The bonding is implemented using a layer of Cotronics Corp. Duralco 132 aluminum-filled, high thermoconductivity epoxy. This epoxy and the roughness particles are applied to an indented region located across the central span of each airfoil. This approach is used to give the same exterior dimensions to the surfaces of all four test vanes, regardless of whether their surfaces are smooth or rough.

A schematic diagram of test turbine vane with uniform rough surfaces is shown in Fig. 2(*a*). The vane with the uniform smaller-sized roughness elements has Praxair T1166F particles, which range in size from 20 to 53 μm. The vane with the uniform larger-sized roughness elements has Praxair NI-914 particles, which range in size from 88 to 149 μm. The vane with variable roughness is shown in Fig. 2(*b*). Four types of different Nickel based powders are used on the pressure side of a test vane, while the suction side is left smooth. Detailed information regarding the nickel powders and surface coverage for the variable rough vane is given in Table 3.

The arrangement of variable rough surface is based on observations of roughened turbine vanes from industrial applications. From these observations, the suction side is more or less uniform in roughness, and remains at or very close to the "as-cast" condition, even after very long operating times. Pressure side roughness, on the other hand, is more variable. Local roughness magnitudes are often the same as on suction side roughness at the leading edge. Local roughness sizes then vary linearly to the full roughness size, which are typically reached at about 40% of the distance along the pressure surface. Thus, differences in surface roughness characteristics between the suction and the pressured sides can be very significant due to the different flow and operating conditions encountered. There is also a considerable scatter in the roughness patterns both in qualitative and quantitative terms that are present on vanes and blades from operating engines. The configuration of variable roughness investigated is one typical configuration, as shown by the data presented in Fig. 2(*b*) and in Table 3.

Table 2 Test vane geometric parameters

True Chord *c*	7.27cm
Axial Chord *cx*	4.85 cm
Pitch *p*	6.35 cm
Span	12.7 cm
Flow turning angle	62.75°

Table 3 Nickel based powders used on the test vane with variable surface roughness on the pressure side

Percentage of the surface distance on the PS Side (starting from LE)	Powder Name	Size (μm)
0 - 10%		0
10% - 20%	NI-105	5-45
20% - 30%	T1166F	20-53
30% - 40%	NI-107	45-106
40% - 100%	NI-914	88-149

2.4 Pressure and Temperature Measurements. As tests are conducted, Validyne Model DP15-46 pressure transducers (with diaphragms rated at 13.8, 34.5, or 344.7 kPa), and calibrated copper-constantan thermocouples are used to sense pressures and temperatures at different locations throughout the facility. A United Sensor PLC-8-KL pitot-static probe with an attached, calibrated Watlow standard type-K copper-constantan thermocouple, and a four-hole conical-tipped pressure probe also with a similar thermocouple are used to sense total pressure, static pressure, and recovery temperature at the inlet and exit of the test section, respectively, during each blow down. Mach numbers, sonic velocities, total temperatures, and static temperatures are determined from these data. The four-hole probe has a tip which is 1.27 mm in diameter, and a stem which is 3.18 mm in diameter. Each port has a diameter of 0.25 mm. The overall response time of the pressure measuring system is about 0.2 s. The conical probe is aligned using two yaw ports placed on either side of the probe. The probe is located downstream of the vane. The position in the streamwise direction is adjustable. As a blow down is underway, it is traversed across a full pitch using a two-axis traversing sled with two Superior Electric synchronous stepper motors, connected to a Superior Electric programmable motion controller and a Superior Electric driver. Commands for the operation of the motion controller are provided by LABVIEW 7.0 software and pass though a serial port after they originate in a Dell Precision 530 PC workstation. Each profile is measured through the wake from minus y/cx locations to positive y/cx locations, and then repeated as the probe is traversed in the opposite direction. The resulting data are subsequently averaged at each wake measurement location.

Voltages from the carrier demodulators and thermocouples are read sequentially using Hewlett-Packard HP44222T and HP44222A relay multiplexer card assemblies, installed in a Hewlett-Packard HP3497A low-speed Data Acquisition/ Control Unit. This system provides thermocouple compensation electronically such that voltages for type T thermocouples are given relative to 0 °C. The voltage outputs from this unit are acquired by the Dell Precision 530 PC workstation through its USB port, using LABVIEW 7.0 software and a GPIB-USB-B adaptor made by National Instruments.

2.5 Longitudinal Turbulence Intensity Measurements. A single, horizontal-type platinum-plated tungsten hot-wire sensor, with a diameter of 12.7 μm and a length of 2.54 mm, is employed to measure the time varying longitudinal component of velocity at the inlet of the test section. The time-averaged longitudinal velocity, and longitudinal turbulence intensity are then determined from these measurements. The measurement location is one axial chord length upstream of the vane leading edge. The hot-wire probe is driven by a Disa 55M10 constant-temperature hot-wire anemometer bridge with an overheat ratio of 1.6. The analog signal from this bridge is then processed using a Dantec 56N20 signal conditioner with a low-pass, anti-aliasing filter set to 100 kHz. The time-varying output voltage signal is then sampled at a 200 kHz rate using a DATEL PCI441D I/O board installed in the Dell Precision 530 PC workstation. During each measurement, 2,000,000 voltage values are sampled over a time period of 10 s. Data are acquired using LABVIEW 7.0 software and then processed further using MATLAB 6.1 software. The entire measurement system, including the hot-wire sensor, is calibrated in the free-stream of the TWT. A Kiel type pressure probe, wall static taps, and a copper-constantan thermocouple are used to measure and determine the total pressure, static pressure, recovery temperature, and velocity at the inlet of the test section as the calibration is conducted.

2.6 Experimental Uncertainties. Uncertainty estimates are based on 95% confidence levels, and determined using procedures described by Kline and McClintock [25] and by Moffat [26]. Mach number uncertainty is 0.002. Uncertainty of temperatures is 0.15 °C. Pressure uncertainty is 0.25 kPa. Uncertainties of $C_p, M_e/M_{e\infty}$, and KE are 0.0013 (0.07), 0.0023 (0.96), and 0.03(0.90), respectively, where typical nominal values of these quantities are given in parenthesis. IAL uncertainty is 0.04 N/cm(0.800 N/cm). Magnitudes of IAL, determined from replicate runs, are always within IAL uncertainty ranges.

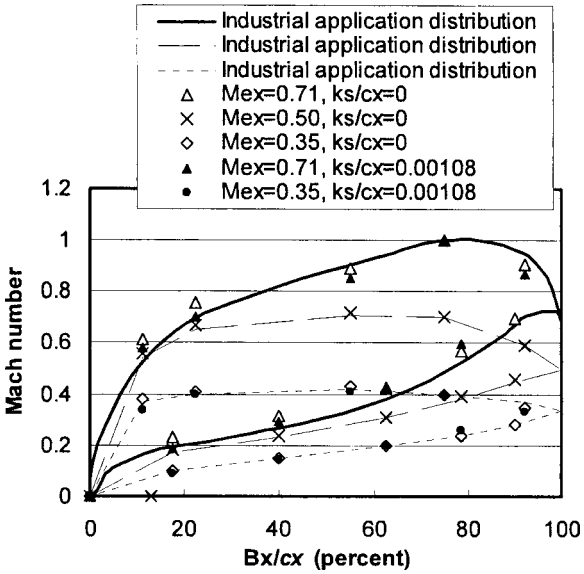

Fig. 3 Mach number distributions along the test vane

3 Experimental Results and Discussion

3.1 Test Section Flow Characteristics and Mach Number Distributions. During each blow-down test, the total pressure, Reynolds number, and turbulence level at the test section inlet are maintained in a continuous and steady fashion for 45 s long time intervals. Such characteristics are not only due to the TWT design, but also to the excellent performance characteristics of the TWT mainstream air pressure regulator and its controller. The total pressure and static pressure show excellent spatial uniformity at the inlet of the test section. Here, total pressure and static pressure values vary by less than 0.5% of mean values as measurements are made at five different pitchwise locations. Magnitudes of inlet turbulence intensity, based on longitudinal velocity fluctuations, are 1.1% for $M_{ex}=0.71$, 1.2% for $M_{ex}=0.50$, and 1.6% for $M_{ex}=0.35$. The measurement location for these values is one chord length upstream of the vane leading edge.

Table 1 gives experimental conditions for the three different operating conditions which are employed in this study. Figure 3 shows the Mach number distributions along the turbine vane pressure side and along the vane suction side for each of these three operating conditions. Each different operating condition is produced by setting a different stagnation pressure at the test section inlet using the TWT mainstream air pressure regulator. Note that the exact same positions of the tailboards and the same flow settings on the bleeding system (shown in Fig. 1) are used for each flow condition. The data shown in Fig. 3 are based upon measurements of total pressure at the test section inlet, and vane mid-span static pressures. These are measured using two different airfoils which are constructed especially for this task: (i) A smooth vane ($k_s/cx=0$), and (ii) a vane with uniform roughness ($k_s/cx=0.00108$). Each of these vanes has five pressure taps on the pressure side, and five pressure taps on the suction side, as well as one pressure tap located on the leading edge at the vane midspan. As shown in Fig. 3, one Mach number distribution employed in this study is transonic on the vane suction side and subsonic on the pressure side, and the other two operating conditions are completely subsonic. Note that a strong adverse pressure gradient is

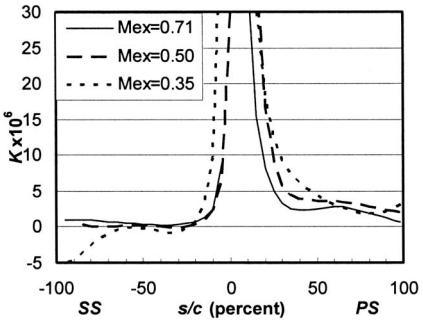

Fig. 4 Distributions of acceleration parameter *K*

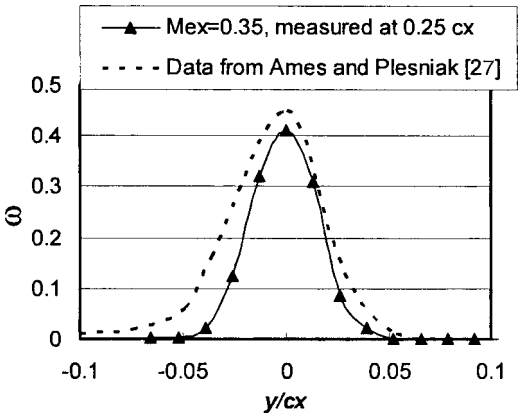

Fig. 5 Comparison of smooth vane wake total pressure loss coefficient profile with similar data from Ames and Plesniak [27]

present on the suction side of the vane when $Bx/cx>0.80$ for $M_{ex}=0.71$. Figure 3 also shows that the Mach number distributions on pressure and suction sides for all three exit Mach numbers are in excellent agreement with data from operating gas turbine engine environments.

Figure 3 also shows that the Mach number distributions for the roughened vane with $k_s/cx=0.00108$ and the smooth vane are in excellent agreement for two of the experimental conditions corresponding to $M_{ex}=0.71$ and $M_{ex}=0.35$. This means that: (i) the roughness has little effect on the airfoil Mach number and surface static pressure distributions, and (ii) the contour shapes of the smooth vane and uniformly roughened vane with $k_s/cx=0.00108$ are the same. This first result is consistent with data from Bammert and Sandstede [9] and Kind et al. [10], who also show that roughness has only small effects on the turbine airfoil pressure distributions. Note that the trailing edge area is not accessible for measurement because static pressure tap tubes cannot be installed in the portion of the vane with such a small trailing edge diameter. However, numerical predictions by Zhang et al. [7] show that static pressures are only slightly different near the trailing edges of symmetric airfoils with smooth and uniformly roughened surfaces.

Figure 4 presents distributions of acceleration parameter K. For each flow condition, considerably higher acceleration parameters are present on the pressure side ($K>2\times10^{-6}$). The resulting acceleration is expected to produce thinning of the turbulent boundary layers accompanied by a suppression of boundary layer turbulence.

3.2 Comparison With Results From Ames and Plesniak. To verify experimental data obtained and procedures employed, a comparison is made with results from Ames and Plesniak [27]. To do this, a total loss coefficient ω is determined, which is defined using

$$\omega=\frac{P_{oi}-P_{oe}}{P_{oi}-P_{se}} \tag{1}$$

The Ames and Plesniak data are taken approximately 0.3 axial chord lengths downstream of a smooth vane with $M_{ex}=0.27$. The vane used by Ames and Plesniak is two times the size of vanes from present study, and has an exit angle of 72.4 deg, compared to an exit angle of 62.75 deg for the present investigation. The present data used for comparison are obtained for $M_{ex}=0.35$ at a measurement location of 0.25 axial chord length downstream of the trailing edge of a smooth vane. Figure 5 shows that the two sets of data have similar magnitudes and similar qualitative distributions. The small quantitative differences are due to slightly different vane configurations, flow conditions, and measurement locations relative to the vane trailing edges. Overall, the agreement between the two data sets provides verification of procedures and results from the present study. Note that no significant freestream losses are present in either study at these experimental conditions because they entail the use of low inlet turbulence intensities and relatively low subsonic Mach numbers.

3.3 Rough Surfaces Measurement and Characterization. Magnitudes of equivalent sandgrain roughness are determined for all surfaces under investigation using procedures described by Van Rij et al. [6]. The first step in this process is determination of detailed surface contour coordinates using a Wyko high-resolution Optical Surface Profilometer. Figure 6(*a*) shows an enlarged image of a portion of the test rough surface which is comprised of nickel powder T1166F, obtained from such optical profilometry data. The image of a rough surface from the pressure side of a turbine vane from a utility power engine is shown in Fig. 6(*b*). This particular sample is obtained from a location on the surface which is located close to the trailing edge area, which is roughened due to surface particulate deposition. The qualitative and quantitative similarity of the two images is apparent, including the distributions, irregularity, nonuniformity, and three-dimensional nature of the roughness elements. Equivalent sand grain roughness size of this real turbine vane surface is about 62.3 μm, which is close to 52.59 μm, the size for the test surface with Nickel powder T1166F. Table 4 also shows the similarity of other surface roughness statistics from the utility power engine turbine vane to test surfaces comprised of Nickel powders T1166F and NI-914.

The second step in the procedure is numerical determination of a modified version of the Sigal and Danberg roughness parameter Λ_s [4–6]. According to van Rij et al. [6], the modified version of Λ_s is defined using

$$\Lambda_s=\left(\frac{S}{S_f}\right)\left(\frac{S_f}{S_s}\right)^{-1.6} \tag{2}$$

where S is the reference area, or the area of the smooth base surface before adding on the roughness, S_f is the total frontal area over the rough surface, and S_s is the windward wetted surface area of all of the roughness elements on the surface. S/S_f is then a roughness density parameter, and S/S_s is a roughness shape parameter.

In the third part of the procedure, with Λ_s known, the ratio of equivalent sandgrain roughness size to mean roughness height, k_s/k, is determined using a correlation for three-dimensional, irregular roughness with irregular geometry and arrangement. According to van Rij et al. [6], k_s/k is given by

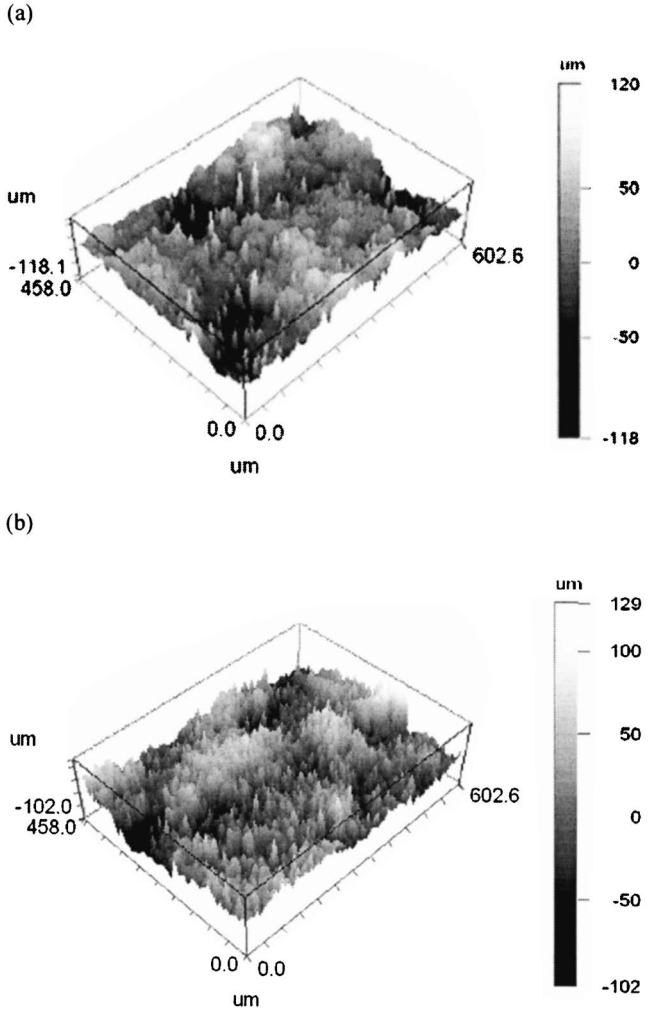

Fig. 6 Three-dimensional Wyko profilometry traces of portions of the rough surfaces. (*a*) Simulated rough surface with small-sized roughness elements. (*b*) Rough surface from the pressure side of a turbine vane with particulate deposition from a utility power engine.

$$\frac{k_s}{k} = \begin{cases} 1.584 \times 10^{-5} \Lambda_S^{5.683} & \Lambda_S \leqslant 7.842 \\ 1.802 \Lambda_S^{0.0304} & 7.842 \leqslant \Lambda_S \leqslant 28.12 \\ 255.5 \Lambda_S^{-1.454} & 28.12 \leqslant \Lambda_S \end{cases} \quad (3)$$

The mean roughness height k is estimated as the distance between the maximum point of the ensemble-average of all of the roughness peaks in any roughness sample, and a base height. Determination of this base location is based on analytic procedures which are also given by Van Rij et al. [6].

With this approach, magnitudes of equivalent sand grain roughness size for the three-dimensional, irregular roughness of the present study are determined. Resulting values are given in Table 4, where each is based on an average of measurements from eight separate profilometry scans of each surface.

3.4 Local Aerodynamic Performance. Here, the effects of surface roughness and exit Mach number on the local wake profiles are presented and discussed. To provide an appropriate standard of comparison, each profile is measured over one complete exit pitch spacing (or one complete exit vane spacing). In addition, the inlet total pressure is always kept constant as different vanes are employed for the same operating condition.

Figures 7 and 8 show the effects of surface roughness on normalized local total pressure losses C_p, normalized local Mach numbers $M_e/M_{e,\infty}$ and normalized local kinetic energy KE for $M_{ex}=0.71$. These data are measured in the wake at 0.25 chord lengths and one axial chord length downstream of vanes, respectively. The different profiles provide information on local wake deficits of total pressure, Mach number, and kinetic energy. Data are given for a smooth vane, and vanes with uniform small-sized roughness ($k_s/cx=0.00108$), uniform large-sized roughness ($k_s/cx=0.00258$), and variable roughness. The inlet total pressure is kept constant at 106 kPa to maintain the same operating condition.

The wake profiles shown in Figs. 7 and 8 are asymmetric. Suction side wakes (at negative y/cx) are thicker than the pressure side wakes (at positive y/cx). The asymmetry in the wake is due to loading on the vane surface, and the past history of the flow. In addition, the growth and development of boundary layers on the suction and pressure sides are different. On the suction side, where local freestream velocities are higher, the boundary layers continue to become thicker up to the trailing edge. The thicker boundary layers then separate from the suction surface of the vane, which affects wake behavior immediately downstream of the trailing edge. In contrast, on the pressure side, boundary layers decrease in thickness in the back section of the vane contour as a result of locally higher flow acceleration. Bammert and Sandstede [9] report data showing the boundary layer on the suction side is considerably thicker than on the pressure side. According to them, wake profile losses are determined more by suction side events by a factor about 2.5–3.5 times compared to events originating near the pressure side.

Figure 7 shows that total pressure losses, Mach number deficits, and deficits of kinetic energy all increase at each y/cx location within the wake as k_s/cx increases, provided the roughness on the surfaces is uniform. The boundary layers along the vane surfaces are thickened as k_s/cx increases, which is accompanied by higher magnitudes of Reynolds stress tensor components, higher magnitudes of local turbulent transport, and higher surface skin friction coefficients. The broader wakes with increased roughness size in Fig. 7 are then the result of: (i) different boundary layer development with various roughness, (earlier laminar-turbulent transition might be caused by surface roughness, as discussed by Stripf et al. [15] and Roberts and Yaras [16].); (ii) augmentations mixing and turbulent transport in the boundary layers which develop along the

Table 4 Characteristics of rough surfaces investigated

Surface	Λ_s	k_s/k	$k(\mu m)$	$k_s(\mu m)$	k_s/cx
Smooth	3020.7	.0026	3.50	.0094	0
Rough Surface with Nickel Powder T1166F	20.1	1.889	27.92	52.59	.00108
Rough Surface with Nickel Powder NI-914	15.4	1.959	64.03	125.19	.00258
Variable Rough Surface				See Fig. 2b	
Turbine vane from a utility power engine	43.5	1.641	40.82	62.30	.00129

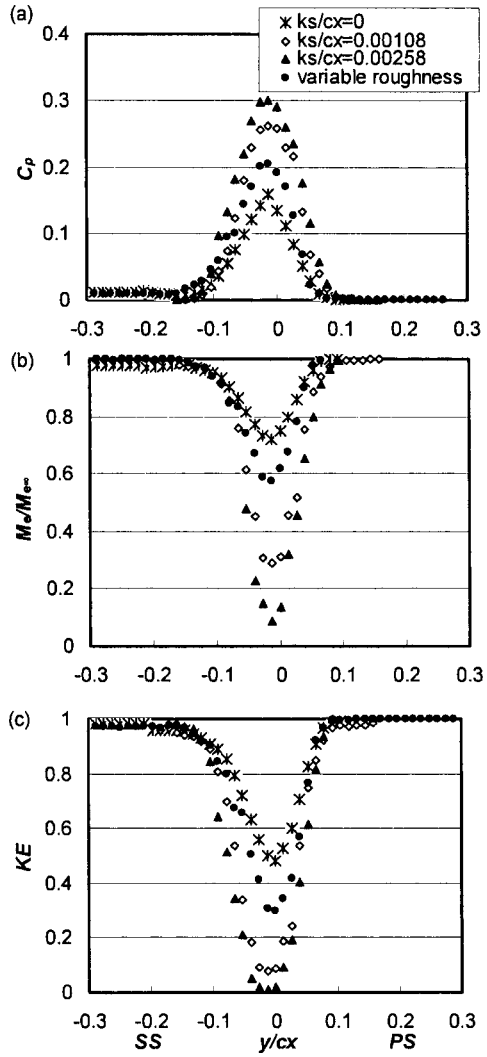

Fig. 7 Profiles measured at 0.25 axial chord length downstream of the test vane for M_{ex}=0.71. (*a*) Normalized local total pressure losses. (*b*) Normalized local Mach numbers. (*c*) Normalized local kinetic energy.

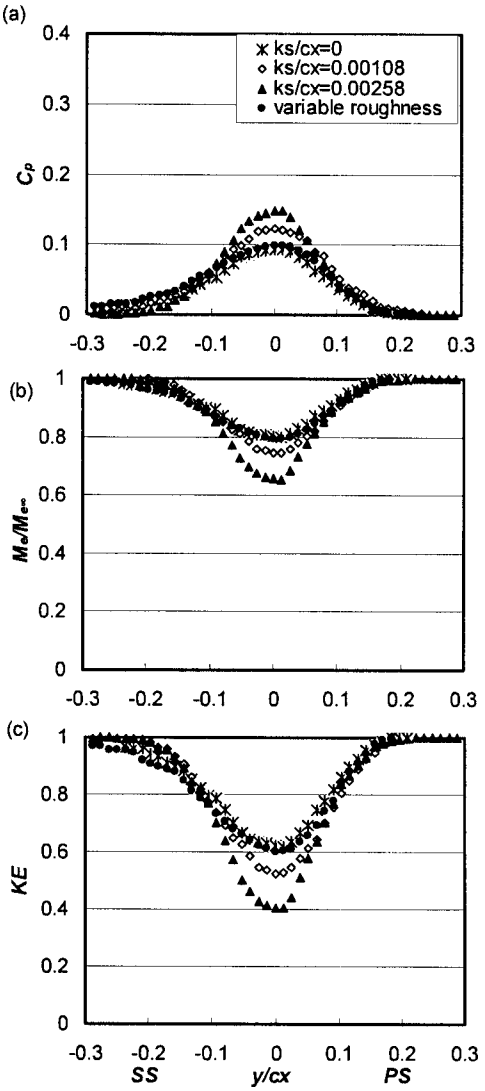

Fig. 8 Profiles measured at one axial chord length downstream of the test vane for M_{ex}=0.71. (*a*) Normalized local total pressure losses. (*b*) Normalized local Mach numbers. (*c*) Normalized local kinetic energy.

roughened vanes; (iii) thicker boundary layers at the trailing edges of the roughened vanes; and (iv) increased turbulent diffusion in the transverse direction within the wake as it advects downstream.

Compared with the results in Fig. 7, the profiles in Fig. 8 (measured one chord length downstream of the vane) are broader (i.e., spread over a wider range of y/cx), with lower peak values. This is mostly a result of transverse turbulent diffusion of streamwise momentum as the wake advects from 0.25 to one axial chord length downstream. Figures 7 and 8 additionally show that increased thickening of the wake is especially apparent as surface roughness size becomes larger. This is especially apparent and more substantial within the wake at negative y/cx values, or downstream of the suction sides of the vanes. In contrast, the effects of surface roughness are much less apparent for positive y/cx values, or downstream of the pressure sides of the vanes. This is especially evident in Fig. 8 since profiles for all three k_s/cx values (0, 0.00108, 0.00258), as well as for the variable roughness vane, are similar for $y/cx > 0.05$. This is partially due to the different growth of boundary layers on the pressure and suction sides for different amounts of surface roughness.

Figures 7 and 8 also include measurements made downstream of the vane with variable roughness shown in Fig. 2(*b*). In most cases, variable surface roughness profile points in Figs. 7 and 8 lie between the profiles measured with $k_s/cx=0$, and $k_s/cx=0.00108$ for $y/cx > -0.1$. This is partially due to different rates of boundary layer development as different levels of roughness are encountered along the vane pressure surface. This gives different magnitudes of boundary layer mixing and losses, and a different wake initial condition near the vane trailing edge, compared to vanes with uniformly roughened surfaces. These changes produced on the vane pressure side appear to have some influence on initial wake behavior downstream of the vane suction side. As a result, suction side wake profiles at $y/cx < 0$ downstream of the vane with a variable rough surface are widened. Thus, suction side wake profiles in Figs. 7 and 8 are also widened somewhat for the vane with variable roughness, even though this vane has a smooth suction side. Overall, the wakes are pushed toward smaller y/cx values as they are advected downstream (i.e., towards the vane suction side), regardless of the level, uniformity, or variability of the roughness along the surfaces of the vanes.

Figures 9 and 10 show the effects of surface roughness on C_p profiles in the wake which are measured one axial chord length downstream of test vanes at M_{ex}=0.50 and 0.35, respectively. From these two figures, the asymmetry, widening and broadening wake with roughness are quite similar to results which are given

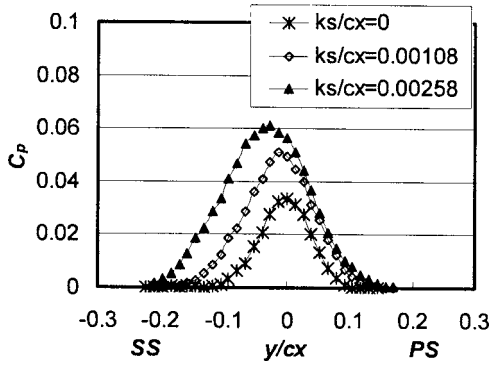

Fig. 9 Normalized local total pressure loss profiles measured at one axial chord length downstream of the test vane for M_{ex} =0.50

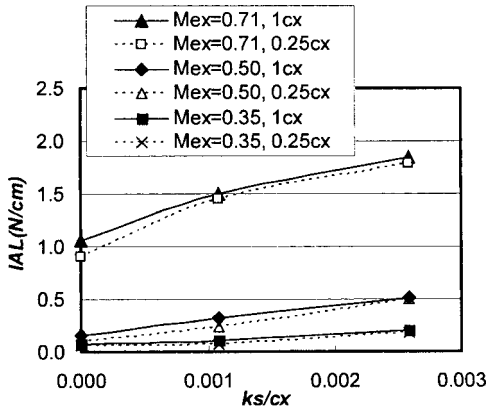

Fig. 11 Comparison of normalized integrated aerodynamic loss as dependent upon the normalized equivalent sand grain roughness size

in Fig. 8(*a*). For example, as the level of surface roughness increases, losses increase substantially at negative y/cx values (i.e., downstream of vane suction sides), whereas smaller variations with changing surface roughness are evident at positive y/cx values (i.e., downstream of vane pressure sides). Comparing results in Figs. 10, 9, and 8(*a*) shows that peak values of total pressure loss coefficients increase dramatically as M_{ex} increases. For example, peak values are approximately 0.03 at M_{ex}=0.35, 0.06 at M_{ex}=0.50, and 0.15 at M_{ex}=0.71. The wakes also become wider as M_{ex} increases. Wider C_p profiles are a result of higher advection speeds, as well as increased diffusion within the wake. The change of the Mach number distribution along the vane for different M_{ex} also affects the pressure gradient imposed on the boundary layer. At higher exit Mach numbers, greater losses are created due to higher rates of turbulence mixing with higher stain rates. Compressibility, which becomes more important at higher exit Mach numbers, also produces additional alterations to the character and development of boundary layers.

Figures 9 and 10 also show wake shifting towards more negative y/cx values with streamwise development. This becomes more substantial as the level of surface roughness increases, or as the exit Mach number decreases. For example, the data in Fig. 9 for M_{ex}=0.50 indicate that the roughened vanes with k_s/cx =0.00108 and k_s/cx=0.00258 have flow deviation angles estimated to be 0.7 and 1.5 deg, respectively. Figure 10 for M_{ex} =0.35 shows that roughness produces even larger deviation angles of approximately 1.3 and 2.9 deg for k_s/cx=0.00108 and k_s/cx =0.00258, respectively. Deviation angles thus appear to increase as M_{ex} decreases or as k_s/cx increases. Larger flow deviations are more apparent at lower exit Mach numbers probably because of earlier flow separation near the suction side trailing edge.

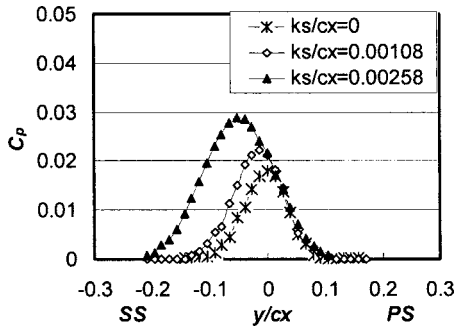

Fig. 10 Normalized local total pressure loss profiles measured at one axial chord length downstream of the test vane for M_{ex} =0.35

3.5 Integrated Aerodynamic Losses. Dimensional magnitudes of Integrated Aerodynamic Loss, IAL, are determined by integrating profiles of $(P_{oi}-P_{oe})$ with respect to y in the transverse flow direction across the wake for one single vane spacing, from $-p/2$ to $p/2$.

$$\mathrm{IAL} = \int_{-p/2}^{p/2} (P_{oi} - P_{oe})dy \tag{4}$$

In the present study, IAL magnitudes are mostly the result of two phenomena. These are: (i) the losses resulting from formation of the boundary layers along the vane surfaces, and (ii) the flow separation, recirculation zone, and wake mixing losses that are initially present just downstream of the vanes.

IAL magnitudes are determined from profiles that are measured 25% of one axial chord length, and one axial chord length downstream of the turbine vane. Such IAL magnitudes are presented in Fig. 11 as dependent upon the normalized equivalent sandgrain roughness size for three exit Mach numbers. The overall trends of the data in this figure illustrate the dominating influences, first, of the Mach number distribution along the airfoil (as designated by exit Mach number), and second, of the surface roughness (as characterized by normalized equivalent sandgrain roughness size). For each value of k_s/cx, dramatic and important IAL magnitude increases are present as higher Mach numbers are present along the airfoil. This is mostly due to higher advection speeds, increased diffusion, and probably earlier laminar to turbulent boundary layer transition of the boundary layers at higher Mach numbers, noting that Reynolds numbers and Mach numbers are not independent in the present study. IAL magnitudes also increase almost linearly as k_s/cx increases for each profile measurement location and for each value of exit Mach number. The IAL differences obtained at each M_{ex} for $1cx$ and $0.25cx$ are relatively small compared to overall IAL loss magnitudes. This is a result of how momentum and turbulence kinetic energy are conserved through the wake. Near the vane trailing edge, most turbulence in the wake is initially produced in the separated and recirculating flow zones, which give the initial condition for wake profile development, as well as initial values of turbulence at the beginning of the wake. As the wake continues to develop downstream, turbulence decays with streamwise distance because turbulence production is less than diffusion and advection. As a result, the shape of momentum deficit changes mostly due to the transverse diffusion of momentum. Overall magnitudes of total pressure deficits and momentum deficits then do not change greatly as the wake is advected in the streamwise direction because not much mean streamwise momentum is converted into turbulence by local shear and turbulence production. Such trends in the present data are consistent with results presented by Mee et al. [28], who suggest that most en-

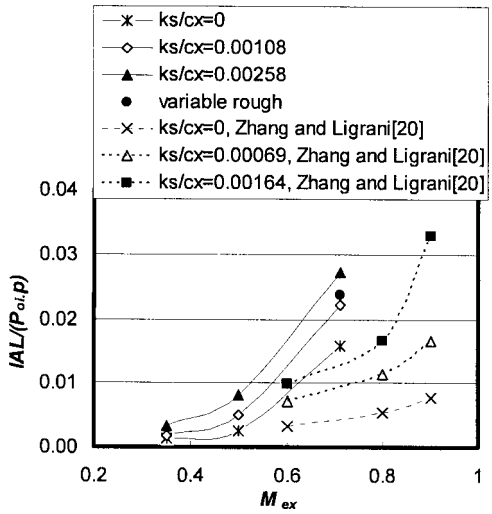

Fig. 12 Comparison of normalized integrated aerodynamic loss magnitudes as dependent upon exit Mach number, and measured one chord length downstream of the airfoils

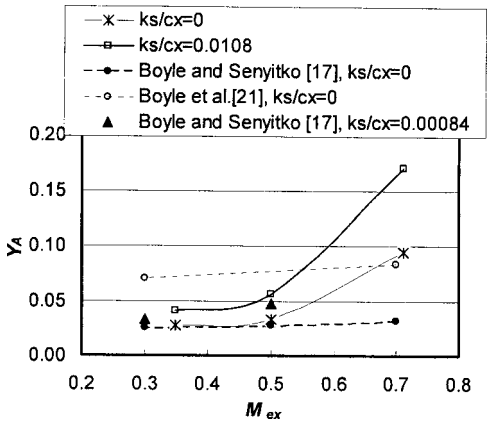

Fig. 13 Comparison of area averaged loss coefficient with Boyle and Senyitko [17], and Boyle et al. [21]

tropy increases take places close to the trailing edge of the airfoils. Additional mixing losses are then only a small fraction of overall loss magnitudes.

IAL data are normalized using the test section passage pitch p and test section inlet stagnation pressure P_{oi} in Fig. 12, which shows how *IAL* data vary with exit Mach number for different values of k_s/cx. IAL values increase as the exit Mach number increases for each value of k_s/cx. Note that dramatic increases in IAL magnitudes are observed as the exit Mach number increases from 0.50 to 0.71. This is due in part to the flow diffusion zone which is present for $Bx/cx > 0.80$ on the suction side of the $M_{\text{ex}} = 0.71$ vane. The overall data trend is consistent with results from Zhang and Ligrani [20], whose data for a symmetric airfoil are included in Fig. 12 and show similar qualitative trends. When compared at the same exit Mach number, the present normalized IAL data for cambered test vanes are then much higher than data obtained downstream of straight symmetric airfoils without flow turning. This is due to different flow diffusion-separation zones, and different flow development over the symmetric and cambered airfoils from different pressure gradients and different amounts of streamline curvature which are imposed on airfoil boundary layers. Such imposed pressure gradients are a result of airfoil shape, the imposed Mach number distribution, and streamline curvature and flow turning in the flow outside of the boundary layers. Overall, these results show that greater losses are present with flow turning and cambered airfoils.

One data point is included in Fig. 12 for the vane with variable roughness. As mentioned, different wake behavior is tied to different rates of boundary layer development (especially on the vane pressure side), different magnitudes of boundary layer mixing and losses, and a different wake initial condition near the vane trailing edge (on both pressure and suction sides), compared to vanes with uniformly roughened surfaces. As a result, the corresponding normalized IAL value in Fig. 12 is between values for the $k_s/cx = 0.00108$ and $k_s/cx = 0.00258$ uniformly roughened vanes for an exit Mach number of 0.71.

3.6 Comparisons With Loss Data From Other Research Groups. Different loss coefficient definitions are generally employed by different research groups. Of these, Boyle and Senyiko [17] and Boyle et al. [21] employ an area averaged loss coefficient, Y_A, in their analysis, which is defined using an equation of the form

$$Y_A = \frac{P_{oi} - P_{oe,A}}{P_{oi} - P_{se,A}} \tag{5}$$

Here, $P_{oe,A}$ and $P_{se,A}$ are area averaged exit total pressure and static pressure, respectively. These are determined using equations given by

$$P_{oe,A} = \int_{-p/2}^{p/2} P_{oe} d(y/p) \tag{6}$$

and

$$P_{se,A} = \int_{-p/2}^{p/2} P_{se} d(y/p) \tag{7}$$

respectively. Boyle and Senyiko [17] employ vanes with 5.18 cm axial chord length and 75 deg flow turning angle. Their data are based on measurements made 0.35 of an axial chord length downstream of their vane. In the same experimental facility, Boyle et al. [21] employ vanes with 4.445 cm axial chord length and approximately 80 deg flow turning angle in their investigation. Figure 13 shows comparisons of their data with results from the present study over a range of exit Mach numbers and different k_s/cx values. These data indicate that higher Y_A losses are generally observed as either exit Mach number or surface roughness increases. Of particular interest is the dramatic increase in present Y_A magnitudes that occurs as the exit Mach number increases from 0.5 to 0.7 for the airfoils with k_s/cx magnitudes of 0 and 0.0108. Note that Y_A magnitudes from smooth vanes from Boyle and Senyiko [17] and Boyle et al. [21] are somewhat different from each other because of different vane configurations and different operating conditions in the two investigations. Such differences also partially account for some of the differences between these data and results from the present investigation. In other cases, the present results show agreement with some of the results from Refs. [17,21].

Kind et al. [10] employ a mass averaged loss coefficient, Y_p in their turbine cascade investigation, which is defined using

$$Y_p = \frac{P_{oi} - P_{oe,m}}{q_{e,m}} \tag{8}$$

where $p_{oe,m}$ and $q_{e,m}$ are mass-averaged exit total pressure, and mass-averaged dynamic pressure, respectively. These two parameters are defined with equations that are given by

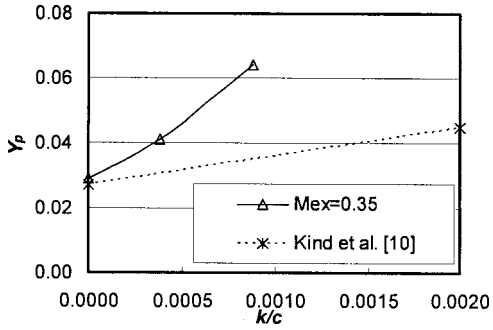

Fig. 14 Comparison of mass averaged loss coefficients with similar results from Kind et al. [10]

$$P_{oe,m} = \frac{\int_{-p/2}^{p/2} \rho u P_{oe} dy}{\rho_\infty u_\infty p} \tag{9}$$

and

$$q_{e,m} = \frac{\int_{-p/2}^{p/2} \rho u q_e dy}{\rho_\infty u_\infty p} \tag{10}$$

respectively. Data from Kind et al. [10] are presented and compared with some data from the present investigation in Fig. 14. Their data are measured 0.4 of an axial chord length downstream of their airfoil. In Fig. 14, Y_p loss coefficient data are given as they vary with normalized mean roughness height k/c since sandgrain roughness height, k_s, is not available from Kind et al. [10]. Y_p loss coefficient results from the present study as well as from Kind et al. [10] increase as the normalized mean roughness height becomes larger. Similar magnitudes of Y_p for the two studies are evident for $k/c=0$ (i.e., smooth vane surfaces). However, differences are evident between the two data sets when $k/c>0$, which are most likely due to different surface roughness characteristics. For example, the Kind et al. [10] roughness with k/c of 0.002, may be comprised of roughness elements with different density compared to ones employed in the present study. Such roughness could thus give different Y_p loss coefficient magnitudes even though mean roughness heights may be comparable.

4 Summary and Conclusions

The effects of surface roughness on the aerodynamic performance of a turbine vane are investigated for three Mach number distributions, one of which results in transonic flow. All three Mach number distributions and the vane configuration match arrangements employed in industrial applications. One smooth vane is employed, along with two other vanes with three-dimensional roughness distributed uniformly over entire vane surfaces. A fourth vane is also employed with roughness of different sizes distributed over the vane surface (i.e., a variable rough surface) whose arrangement is based on observations of roughened turbine vanes from industrial applications. All four turbine vanes have the same shape and exterior dimensions. This is verified for the smooth vane and the vane with uniform $k_s/cx=0.00108$ roughness since the same Mach number distribution is present with each.

The nonuniform, irregular, three-dimensional roughness on the tested vanes is employed to match the roughness which exists on operating turbine vanes and blades subject to extended operating times with significant particulate deposition on the surfaces. This is verified by detailed three-dimensional optical profilometry traces and rough surface statistics (such as equivalent sandgrain roughness size) which are similar for the roughness from a power engine turbine blade and the test surfaces employed in this study.

Total pressure losses, Mach number deficits, and deficits of kinetic energy all increase at each y/cx location within the wake as k_s/cx increases, regardless of the level, uniformity, or variability of the roughness along the surfaces of the vanes. The wakes also become broader with increased roughness size or with increased exit Mach number M_{ex} due to higher advection velocities, augmentations of mixing and turbulent transport, thicker boundary layers, earlier laminar-turbulent transition and increased turbulent diffusion. Peak values of total pressure loss coefficients also increase dramatically as M_{ex} increases. In general, these profiles are asymmetric because the effects of surface roughness are much less apparent for positive y/cx values, downstream of the pressure sides of the vanes. This is due to different loading, different boundary layer growth, and different susceptibility to flow separation on the different vane surfaces, which also causes the suction side wakes (at negative y/cx) to be thicker than the pressure side wakes (at positive y/cx). Overall, the wakes are pushed toward smaller y/cx values as they are advected downstream (i.e., towards the vane suction side), regardless of the level, uniformity, or variability of the roughness along the surfaces of the vanes. Aside from this, the data from a vane with variable surface roughness show different quantitative and qualitative trends compared to profiles measured downstream of vanes with roughness spread uniformly over the surfaces. This is partially due to different rates of boundary layer development as different levels of roughness are encountered along the vane pressure surface.

For each value of k_s/cx, dramatic and important IAL magnitude increases are present as higher Mach numbers are present along the airfoil. IAL magnitudes also increase almost linearly as k_s/cx increases for each profile measurement location and for each value of exit Mach number. When the exit Mach number is 0.71, the normalized IAL value for the variable roughened vane is between values for the $k_s/cx=0.00108$ and $k_s/cx=0.00258$ uniformly roughened vanes. In contrast, the IAL differences obtained at each M_{ex} for $1cx$ and $0.25cx$ are relatively small compared to overall IAL loss magnitudes. This is because not much mean streamwise momentum is converted into turbulence by local shear and turbulence production as the wake is advected in the streamwise direction. When compared at the same exit Mach number, the present normalized IAL data for cambered test vanes are much higher than data obtained downstream of straight symmetric airfoils without flow turning. Overall, this means that greater losses are present with flow turning and cambered airfoils, than with symmetric airfoils.

Magnitudes of area-averaged loss coefficients Y_A generally increase as either exit Mach number or equivalent sandgrain roughness size increases. The increases in Y_A magnitudes are especially substantial as the exit Mach number increases from 0.5 to 0.7 for the smooth vane and the uniformly roughened vane with $k_s/cx=0.0108$. Mass-averaged loss coefficients Y_p show similar trends, since they also increase as normalized mean roughness height becomes larger for a particular value of vane exit Mach number.

Acknowledgment

The research reported in this paper was sponsored by the National Science Foundation (NSF Grant No. CTS-0086011). Dr. Stefan Thynell and Dr. Richard Smith were the NSF program monitors. The authors also acknowledge Dr. Mike Blair of Pratt and Whitney Corporation, Dr. Hee-Koo Moon of Solar Turbines, Inc., Dr. Ed North, Dr. Ihor Diakunchak of Siemens-Westinghouse Corp., and personnel from Pratt and Whitney – Canada Corporation for guidance and suggestions on this research effort, and for providing roughened turbine vane hardware from engines for analysis and comparison. The authors also thank Dr. Forest Ames of the University of North Dakota, Dr. Robert Boyle of NASA Glenn Research Center for their helpful and valuable suggestions on many details of the present research. Atem Khalatov of the Ukrainian Academy of Sciences is also acknowledged for several suggestions he provided on the effort.

Nomenclature

Bx = normal coordinate measured from vane leading edge
c = true chord length
cx = axial chord length
C_p = local total pressure coefficient, $(P_{oi}-P_{oe})/P_{oi}$
IAL = integrated aerodynamic losses
M_e = exit local Mach number
$M_{e,\infty}$ = exit free-stream Mach number
k = roughness height
K = dimensionless acceleration parameter, $(v/U_\infty^2)(dU_\infty/ds)$
KE = normalized local kinetic energy, $(P_{oe}-P_{se})/(P_{oe}-P_{Se})_\infty$
k_s = equivalent sand grain roughness
p = passage pitch
P_o = stagnation pressure
P_{oe} = exit local stagnation pressure
$P_{oe,m}$ = mass averaged exit stagnation pressure
$P_{oe,\infty}$ = exit freestream stagnation pressure
$P_{oe,A}$ = area averaged exit total pressure
$P_{se,A}$ = area averaged static pressure
P_{se} = exit local static pressure
P_{oi} = inlet stagnation pressure
PS = pressure side
q_e = exit local dynamic pressure
$q_{e,m}$ = exit mass-weighted dynamic pressure
s = blade surface length from leading edge of the vane
S = rough surface flat reference area
S_f = total roughness frontal area
S_s = total roughness windward wetted surface area
SS = suction side
u = exit local streamwise velocity
U_∞ = freestream velocity over the vane surface
v = kinematic viscosity
x = linear distance from vane trailing edge in direction of vane trailing edge camber line
y = normal coordinate measured from line tangent to vane trailing edge camber line
Y_A = area averaged loss coefficient used by Boyle et al. [17]
Y_P = mass averaged loss coefficient used by Kind et al. [10], $(P_{oi}-P_{oe,m})/q_{e,m}$
Λ_s = Sigal and Danberg roughness parameter
ω = total pressure loss coefficient used by Ames and Plesniak [27],$(P_{oi}-P_{oe})/(P_{oi}-P_{se})$
ρ = exit local density

Subscripts

A = area-averaged
e = exit
M = mass-averaged
∞ = freestream

References

[1] Nikuradse, J., 1933, "Laws of Flow in Rough Pipes," NACA TM 1292, National Advisory Committee on Aeronautics.
[2] Schlichting, H., 1936, "Experimental Investigation of the Problem of Surface Roughness," NACA TM-832, National Advisory Committee on Aeronautics.
[3] Coleman, H. W., Hodge, B. K., and Taylor, R. P., 1984, "A Re-Evaluation of Schlichting's Surface Roughness Experiment," ASME J. Fluids Eng., **106**, pp. 60–65.
[4] Sigal, A., and Danberg, J. E., 1990, "New Correlation of Roughness Density Effect on Turbulent Boundary Layer," AIAA J., **28**, pp. 554–556.
[5] Sigal, A., and Danberg, J. E., 1988, "Analysis of Turbulent Boundary Layer Over Roughness Surface With Application to Projectile Aerodynamics," Amy Ballistic Research Lab, Aberdeen Proving Grounds MD, Technical Report BRL-TR-2977.
[6] Van Rij, J. A., Belnap, B. J., and Ligrani, P. M., 2002, "Analysis and Experiments on Three-Dimensional, Irregular Surface Roughness." ASME J. Fluids Eng., **124**, pp. 1–7.
[7] Zhang, Q., Lee, S. W., and Ligrani, P. M., 2003, "Determination of Rough-Surface Skin Friction Coefficients From Wake Profile Measurements," Exp. Fluids, **35**, pp. 627–635.
[8] Bammert, K., and Sandstede, H., 1975, "Influence of Manufacturing Tolerances and Surface Roughness of Blades on the Performance of Turbines," ASME Paper No. 75-GT-35.
[9] Bammert, K., and Sandstede, H., 1980, "Measurements of the Boundary Layer Development Along a Turbine Blade With Rough Surfaces." ASME J. Eng. Power, **102**, pp. 978–983.
[10] Kind, R. J., Serjak, P. J., and Abbott, M. W. P., 1996, "Measurements and Prediction of the Effects of Surface Roughness on Profile Losses and Deviation in a Turbine Cascade," ASME Paper No. 95-GT-203.
[11] Bogard, D. G., Schmidt, D. L., and Tabbita, M., 1998, "Characterization and Laboratory Simulation of Turbine Airfoil Surface Roughness and Associated Heat Transfer," ASME J. Turbomach., **120**, pp. 337–342.
[12] Abuaf, N., Bunker, R. S., and Lee, C. P., 1998, "Effects of Surface Roughness on Heat Transfer and Aerodynamics Performance of Turbine Airfoils," ASME J. Turbomach., **120**, pp. 522–529.
[13] Leipold, R., Boese, M., and Fottner, L., 2000, "The Influence of Technical Surface Roughness Caused by Precision Forging on the Flow Around a Highly Loaded Compressor Cascade," ASME J. Turbomach., **122**, pp. 416–425.
[14] Sitaram, N., Govardhan, M., and Murali Krishna, V. T., 1999, "Loss Reduction by Means of Two-Dimensional Roughness Elements on the Suction Surface of a Linear Turbine Rotor Cascade, Flow, Turbul. Combust., **62**, pp. 227–248.
[15] Stripf, M., Schulz, A., and Wittig, S., 2004, "Surface Roughness Effects on External Heat Transfer of a HP Turbine Vane," *Proceedings of ASME Turbo Expo 2004*, GT2004-53114.
[16] Roberts, S. K., and Yaras, M. I., 2004, "Boundary-layer Transition Over Rough Surfaces With Elevated Free-stream Turbulence," *Proceedings of ASME Turbo Expo 2004*, GT2004-53668.
[17] Boyle, R. J., and Senyitko, R. G., 2003, "Measurements and Predictions of Surface Roughness Effects on Turbine Vane Aerodynamics," *Proceedings of ASME Turbo Expo 2003*, GT-2003-38580.
[18] Zhang, Q., Lee, S. W., and Ligrani, P. M., 2004, "Effects of Surface Roughness and Turbulence Intensity on the Aerodynamic Losses Produced by the Suction Surface of a Simulated Turbine Airfoil," ASME J. Fluids Eng., **126**, pp. 257–265.
[19] Zhang, Q., Lee, S. W., and Ligrani, P. M., 2004, "Effect of Surface Roughness and Freestream Turbulence on the Wake Turbulence Structure of a Symmetric Airfoil," Phys. Fluids, **16**, pp. 2044–2053.
[20] Zhang, Q., and Ligrani, P. M., 2004, "Effects of Mach Number and Surface Roughness on the Aerodynamic Losses of a Symmetric Transonic Turbine Airfoil," J. Propul. Power, **20**, pp. 1117–1125.
[21] Boyle, R. J., Luci, B. L., Verhoff, V. G., Camperchioli, W. P., and La, H., 1998, "Aerodynamics of a Transitioning Turbine Stator Over a Range of Reynolds Numbers," ASME Paper 98-GT-285.
[22] Boyle, R. J., 2004, private communication.
[23] Jackson, D. J., Lee, K. L., Ligrani, P. M., Johnson, P. D., 2000, "Transonic Aerodynamics Losses due to Turbine Airfoil, Suction Surface Film Cooling," ASME J. Turbomach., **122**, pp. 317–326.
[24] Furukawa, T., and Ligrani, P. M., 2002, "Transonic Film Cooling Effectiveness From Shaped Holes on a Simulated Turbine Airfoil," J. Thermophys. Heat Transfer, **16**, pp. 228–237.
[25] Kline, S. J., and McClintock, F. A., 1953, "Describing Uncertainties in Single Sample Experiments," Mech. Eng. (Am. Soc. Mech. Eng.), **75**, pp 3–8.
[26] Moffat, R. J., 1988, "Describing the Uncertainties in Experimental Results," Exp. Therm. Fluid Sci., **1**, pp. 3–17.
[27] Ames, F. E., and Plesniak, M. W., 1997, "The Influence of Large-Scale High-Intensity Turbulence on Vane Aerodynamic Losses, Wake Growth, and the Exit Turbulence Parameters," ASME J. Turbomach., **119**, pp. 182–192.
[28] Mee, D. J., Braines, N. C, Oldfield, M. L. G., and Dickens, T. E., 1992, "An Examination of the Contributions to Loss on a Transonic Turbine Blade in Cascade," ASME J. Turbomach., **114**, pp. 155–162.